



# In situ analyses of crystallization behavior of 1,2,3-tripalmitoyl glycerol under static and dynamic thermal conditions

Laura Bayés-García<sup>1</sup> · Jorge Macridachis<sup>1</sup> · Teresa Calvet<sup>1</sup> · Kiyotaka Sato<sup>2</sup>

Received: 25 July 2023 / Accepted: 6 April 2024 / Published online: 1 May 2024  
© The Author(s) 2024

## Abstract

The crystallization behavior of 1,2,3-tripalmitoyl glycerol or PPP using differential scanning calorimetry (DSC), thermo-optical polarized light microscopy and in situ synchrotron radiation X-ray diffraction (SR-XRD) techniques was precisely examined under static isothermal and dynamic thermal treatments, and the results were compared with preceding studies. PPP was rapidly ( $15\text{ }^{\circ}\text{C min}^{-1}$ ) cooled to target temperatures (from 40 to  $59\text{ }^{\circ}\text{C}$ ) to determine the precise moment at which crystallization was initiated. Once crystallization ceased, polymorphic transformation and melting were analyzed during subsequent heating.  $\alpha$  form was crystallized during isotherms from 40 to  $46\text{ }^{\circ}\text{C}$ , temperature at which it coexisted with  $\beta'$  phase. The latter was solely formed from 47 to  $53\text{ }^{\circ}\text{C}$ , and polymorphic crystallization was directed to obtain exclusively most stable  $\beta$  at  $54\text{ }^{\circ}\text{C}$  and higher temperatures. Nucleation time values for the  $\alpha$ ,  $\beta'$  and  $\beta$  polymorphs exhibited exponential growth type, and a good correlation was found between data obtained by DSC and SR-XRD. Dynamic experiments were based on the use of high ( $15\text{ }^{\circ}\text{C min}^{-1}$ ), intermediate ( $2\text{ }^{\circ}\text{C min}^{-1}$ ) and low ( $0.5$  and  $0.1\text{ }^{\circ}\text{C min}^{-1}$ ) cooling and heating rates. Thermo-optical polarized light microscopy experiments also provided valuable information on microstructural changes occurring during polymorphic modifications. Less stable forms predominated at high cooling rates, whereas lower velocities led the polymorphic crystallization to obtain more stable forms.

**Keywords** Tripalmitin · Polymorphism · Nucleation kinetics · Triacylglycerol · DSC · X-ray diffraction

## Introduction

Natural lipids are multicomponent systems in which triacylglycerol (TAG) molecules represent the major fraction. The physical properties of lipid-based products from different industrial sectors (e.g., pharmacy, cosmetics, food) are strongly determined by TAG crystals, which are formed during manufacturing processes [1]. This means that an adequate control of industrial operations to obtain products with specific quality standards relies on an in-depth knowledge about the crystallization behavior of TAGs, which in turn passes through a good understanding of main aspects, such as molecular and crystal structures, solidification and

transformation processes, and the rheological and textural behavior resulting from fat crystal networks [2]. Specific solidification properties of TAGs, such as crystallization rate, crystal size and morphology, and network crystallinity, are all interrelated and strongly influenced by polymorphism [3]. Therefore, one of the main challenges of industrial crystallization processes is setting the conditions to achieve the most suitable polymorphic forms to each specific application and prolonging shelf-life to the maximum possible extent.

Fully saturated monoacid TAGs are not usually major components in edible fats and oils, but may determine the crystallization and melting behavior due to their high-melting properties. More concretely, these TAGs tend to crystallize first, and the solid material formed promotes the heterogeneous nucleation of lower-melting components. This so-called seeding effect is of practical value for the design of faster crystallization processes and, among the existing tri-saturated monoacid TAGs, 1,2,3-tripalmitoyl glycerol or PPP has proved to be suitable as a crystallization modifier of natural lipids such as palm oil, in which it is naturally

✉ Laura Bayés-García  
laurabayes@ub.edu

<sup>1</sup> Departament de Mineralogia, Petrologia i Geologia Aplicada, Facultat de Ciències de La Terra, Universitat de Barcelona, Martí i Franquès, S/N, 08028 Barcelona, Spain

<sup>2</sup> Faculty of Applied Biological Science, Hiroshima University, Higashi-Hiroshima 739-8528, Japan

present [4], and oleic-rich blends including vegetable oils from diverse sources [5–7].

The crystallization and phase transformation kinetics of PPP under isothermal conditions has been extensively investigated. Sato and Kuroda [8] first determined the rates of melt crystallization and phase transformation of PPP polymorphs  $\alpha$ ,  $\beta'$  and  $\beta$  with optical microscopy. Laboratory-scale X-ray diffraction (XRD) allowed the polymorphic identification, but experiments were carried *ex situ* at a fixed temperature after the crystallization ceased. Later, Kellens' group exhaustively examined the polymorphic behavior of PPP and isolated the different polymorphs by applying tailored cooling and isothermal protocols, which were monitored by differential scanning calorimetry (DSC) and synchrotron radiation X-ray diffraction (SR-XRD) methods [9]. One of their conclusions was, disagreeing with Hagemann's previous work [10, 11], the non-existence of submodifications of a same polymorph for PPP, that is multiple  $\beta'$  or  $\beta$  forms. By contrast, they supported the idea that variations observed between the polymorphic forms may be understood as differences in crystallinity and crystal perfection. The same authors later carried out isothermal crystallization experiments of PPP at different temperatures with DSC and laboratory-scale XRD [12]. However, XRD experiments were again performed *ex situ* by subjecting PPP to the thermal treatment in a hot stage, and then, XRD patterns were obtained at room temperature.

The temperature variations employed in the above previous studies could lead to some deviations compared to the results obtained through *in situ* experimental procedures. Kellens' group later studied the morphology and kinetics of crystallization of PPP with optical polarized microscopy under analogous conditions [13]. They analyzed the isothermal crystallization of the different polymorphs by cooling from the melt to target temperatures and determined their nucleation and crystal growth rates. Crystal structures were identified through the melting behavior of the samples when heated after complete crystallization. However, some differences were noticed compared to the DSC results previously obtained [12] which, according to authors, were in part due to the sample setting in two dimensions between the microscope glass plates, which obstructed the  $\beta$  crystallization process.

In a successive study performed by Stapley et al. [14], the authors stated that the differences between microscopy and DSC data could also be attributed to the lack of natural convection currents, which may even occur in a DSC pan, and that may strongly influence and accelerate the  $\beta$  formation. In this research, Stapley and co-authors developed a novel algorithm for image analysis and, combined with hot stage microscopy, they applied it to the isothermal crystallization of PPP, and compared the results obtained with those previous of Kellens' group [12]. Additional data

were obtained by MacNaughtan et al. [15], who reported on the isothermal crystallization of PPP, SSS (1,2,3-tristearoyl glycerol) and their mixtures by mainly using DSC. They identified polymorphs by the subsequent melting of samples, and wide-angle XRD information was used in some cases for confirmation. Then, induction times were not based on the first detectable signs of crystallization, but determined by fitting the entire crystallization DSC curve to the Avrami equation.

Despite of extensive research on the polymorphic behavior of PPP, the use of *in situ* techniques enabling to monitor the crystallization and phase transformation processes is still lacking. The use of laboratory-scale XRD techniques is often insufficient to precisely determine the highly complex polymorphic behavior exhibited by TAGs, as the exposure times required are longer than those needed when synchrotron radiation is employed.

In the present work, we studied the crystallization behavior of PPP under isothermal and when subjected to varied cooling and heating rates by mainly using DSC and SR-XRD. The synchrotron radiation technique allowed us to precisely monitor induction time for PPP crystallization under static conditions at fixed temperatures, and also to follow complex polymorphic phenomena when subjected to rapid cooling and heating rates under dynamic conditions.

## Materials and methods

### Materials

1,2,3-dipalmitoyl glycerol (PPP) (purity > 99%) was purchased from Larodan AB (Solna, Sweden) and used without further purification.

### Differential scanning calorimetry

Differential scanning calorimetry (DSC) experiments were conducted at atmospheric pressure by using a Perkin Elmer DSC-8000 and a Perkin Elmer Diamond (Perkin Elmer, Waltham, MA, USA). The DSC curves obtained by the two calorimeters were completely comparable. Samples (4.000–4.600 mg) were weighed into 50  $\mu\text{m}$  aluminum pans, and an empty pan was used as a reference. Both instruments were calibrated according to indium's and decane's standard melting temperatures and enthalpies. Dry nitrogen was used as purge gas in the DSC measurement chamber, at a flow rate of 20  $\text{cm}^3 \text{min}^{-1}$  in both apparatuses. DSC curves were analyzed using Pyris software to obtain  $T_{\text{peak}}$  and  $T_{\text{onset}}$  (or  $T_{\text{end}}$ ) transition temperatures.  $T_{\text{peak}}$  corresponded to the temperature at peak top positions, whereas  $T_{\text{onset}}$  (or  $T_{\text{end}}$ ) was defined as the temperature at intersections between baselines and tangents at inflection points of the initial (or final) peak

slopes. The same methodology was applied to determine onset and peak top values for nucleation time ( $t_{\text{onset}}$  and  $t_{\text{peak}}$ , respectively) at the different experimental conditions examined.

PPP was subjected to isothermal and dynamic DSC experiments. As to isothermal programs, samples were rapidly cooled ( $15\text{ }^{\circ}\text{C min}^{-1}$ ) from the melt to target temperatures from 40 to  $59\text{ }^{\circ}\text{C}$ , kept until complete crystallization and afterward heated at an intermediate rate of  $2\text{ }^{\circ}\text{C min}^{-1}$  to monitor subsequent polymorphic transformation and/or final melting. By contrast, dynamic thermal treatments consisted of cooling molten PPP samples and reheating them thereafter at varied rates as follows: cooling-heating at  $15\text{ }^{\circ}\text{C min}^{-1}$ , cooling-heating at  $2\text{ }^{\circ}\text{C min}^{-1}$ , cooling-heating at  $0.5\text{ }^{\circ}\text{C min}^{-1}$ , and cooling at  $0.1\text{ }^{\circ}\text{C min}^{-1}$  and heating at  $2\text{ }^{\circ}\text{C min}^{-1}$ . A minimum of three independent measurements were conducted for all samples and the results were evaluated for random uncertainty with a 95% threshold of reliability using the Student's method.

### Synchrotron radiation X-ray diffraction

Synchrotron radiation X-ray diffraction (SR-XRD) was employed in order to determine the precise instant at which crystallization took place for isothermal analyses at all experimental conditions, and also to follow complex polymorphic crystallization and transformation occurring during dynamic temperature processes at the highest rate of  $15\text{ }^{\circ}\text{C min}^{-1}$ . Experiments were conducted on beamline BL11-NCD-SWEET at the ALBA synchrotron (Cerdanyola del Vallès, Barcelona, Spain) at  $12.4\text{ keV}$ . X-ray scattering data were collected on a Pilatus 1 M detector with a pixel size of  $172\text{ }\mu\text{m} \times 172\text{ }\mu\text{m}$  for the small-angle X-ray diffraction (SAXD) data, and on a LX255-HS Rayonix detector with a pixel size of  $88\text{ }\mu\text{m} \times 88\text{ }\mu\text{m}$  for the wide-angle X-ray diffraction (WAXD) data. Sample-detector distances were 2.7 m and 0.1 m for SAXD and WAXD detectors, respectively. The temperature of the sample was controlled by a Linkam stage.

The sample was placed in an aluminum sample cell with a Kapton film window. The q-axis calibration was obtained by measuring silver behenate for SAXD and  $\text{Cr}_2\text{O}_3$  for WAXD. The program pyFAI [16] was used to integrate the 2D SAXD and 2D WAXD into the 1D data.

### Laboratory-scale X-ray diffraction

Laboratory-scale XRD measurements were carried out at the facilities of the scientific and technological centers of the University of Barcelona (CCiTUB) for intermediate and low cooling/heating rates of 2, 0.5 and  $0.1\text{ }^{\circ}\text{C min}^{-1}$ . A PANalytical X'Pert Pro MPD powder diffractometer equipped with a hybrid monochromator and a PIXcel detector was used.

The equipment operated with Debye–Scherrer transmission and temperature control was achieved through an Oxford Cryostream Plus 220 V.

The samples were introduced in a 1 mm diameter Lindemann glass capillary, which was rotated about its axis in the course of the experiment to minimize preferential crystalline orientation. The step size was  $0.013^{\circ}$  from  $1^{\circ}$  to  $28^{\circ} 2\theta$ , and the measuring time 150 s per step. Diffraction data were analyzed with X'Pert Highscore V2.2e software.

### Thermo-optical polarized light microscopy

Thermo-optical polarized light microscopy (TOPLM) experiments for samples subjected to dynamic thermal treatments was carried out by using a Nikon Eclipse 50iPol Microscope with a Linkam THMSG-600 stage attached. The system was coupled to an LNP liquid nitrogen cooling system and a TMS94 temperature controller. To visually analyze the sample behavior detected by DSC and XRD analyses, images were captured at different time intervals using a Nikon Digital Camera DXM1200F and Linksys 32 software.

PPP was melted after set on a glass slide, and then, a coverslip was placed on top of the sample. The same was then lightly tapped in order to remove air bubbles. Experiments were performed in duplicate.

## Results and discussion

The relatively simple polymorphism of PPP, which basically exhibits  $\alpha$ ,  $\beta'$  and  $\beta$  forms, all having a double chain-length structure, results from the equivalent fatty acid substituents at the three *sn*- positions of the glycerol group. Long- and short-spacing values for main polymorphic forms of PPP identified in the present work are shown in Table 1.

The occurrence of several  $\beta'$  forms with different subcell packing and melting points has been suggested in monoacid saturated TAGs, such as PPP or 1,2,3-tristearoyl glycerol (SSS) [11], but it is still unclear if in some cases these variations are related to subtle differences in crystalline perfection and crystallinity rather than to significant changes in the molecular arrangement [17].

Recent work on monoacid TAGs based on stearic (S), palmitic (P), miristic (M), and lauric (L) fatty acids (with

**Table 1** Long- and short-spacing values for main polymorphic forms of PPP

	Sub- $\alpha$	$\alpha$	$\beta'$	$\beta$
Long spacing/nm	4.5	4.5	4.2	4.1
Short spacing/nm	0.41; 0.38	0.41	0.43; 0.42; 0.39	0.46; 0.39; 0.37

18, 16, 14, and 12 carbon atoms in their chain, respectively) showed that distinct thermal treatments and starting polymorphs ( $\alpha$  or  $\beta'$ ) led to diverse  $\beta$  forms with similar subcell structure during polymorphic transformations [18]. Since further research is still needed for a better characterization of different  $\beta'$  and  $\beta$  submodifications in monoacid TAGs, these forms will be simply referred to as  $\beta'$  and  $\beta$  in this work.

The nucleation time at different crystallization temperatures was determined for main  $\alpha$ ,  $\beta'$  and  $\beta$  polymorphs. As described further on, least stable sub- $\alpha$  form (see Table 1) was only detected by SR-XRD, and obtained from  $\alpha$  form through a  $\alpha \rightarrow$  sub- $\alpha$  polymorphic transformation when PPP was cooled to sub-zero temperatures at high rates of  $15\text{ }^{\circ}\text{C min}^{-1}$  during dynamic experiments, that is when a sufficient amount of metastable  $\alpha$  phase was formed.

### PPP crystallization under static conditions

Isothermal polymorphic crystallization of PPP was evaluated at 20 different temperatures between 40 and  $59\text{ }^{\circ}\text{C}$  (both included and at every  $^{\circ}\text{C}$ ) after rapid cooling ( $15\text{ }^{\circ}\text{C min}^{-1}$ ) to determine the precise moment at which metastable  $\alpha$ ,  $\beta'$  and/or most stable  $\beta$  forms were firstly detected. DSC and SR-XRD were, therefore, used and the results obtained through the two techniques were compared, but also contrasted with previous work [12].

Nucleation time (onset and peak top values) for the polymorphic crystallization of PPP at the different target temperatures determined by DSC are displayed in Table 2. Additionally, Fig. 1 shows the DSC curves of isothermal crystallization for selected temperatures of 42, 46, 48 and  $55\text{ }^{\circ}\text{C}$  (Fig. 1a), and polymorphic transformation and/or final melting observed during subsequent heating at  $2\text{ }^{\circ}\text{C min}^{-1}$  (Fig. 1b). These temperatures were chosen as example cases for the polymorphic crystallization of the different phases, as it will be next described.

One may note that the  $t_{\text{onset}}$  and  $t_{\text{peak}}$  values displayed in Table 2 do not correspond to the values which can be extracted from the peak positions of the DSC events shown in Fig. 1a. The reason is that the time shown in Fig. 1a also includes the time needed to cool the sample from the melt ( $80\text{ }^{\circ}\text{C}$ ) to each crystallization temperature (within 2.4 and 3.7 min). Then, in order to determine each nucleation time (onset and peak top values displayed in Table 2), a correction which considered the time employed to cool PPP was applied. As expected, nucleation time increased significantly as crystallization temperature increased from 40 to  $59\text{ }^{\circ}\text{C}$  (see Table 2). However, associated errors became also meaningfully more important when PPP was crystallized at higher temperatures, due to a more relevant value dispersion which involved the performance of a higher amount of DSC experiments.

**Table 2** DSC onset and peak top values of nucleation time for isothermal crystallization of PPP, and number of measurements performed at the different temperatures between 40 and  $59\text{ }^{\circ}\text{C}$ .  $T_c$  means crystallization temperature

$T_c/^{\circ}\text{C}$	$t_{\text{onset}}/\text{min}$	$t_{\text{peak}}/\text{min}$	No. measurements
40	$-0.5 \pm 0.2^*$	$-0.3 \pm 0.2^*$	3
41	$0 \pm 0.2$	$0.1 \pm 0.3$	3
42	$\pm 0.2$	$0.2 \pm 0.2$	3
43	$0.1 \pm 0.3$	$0.4 \pm 0.3$	3
44	$0.3 \pm 0.2$	$1.1 \pm 0.5$	3
45	$1.2 \pm 1.3$	$2.6 \pm 1.8$	4
46	$2.0 \pm 1.1$	$3.4 \pm 2.1$	3
47	$2.6 \pm 1.8$	$4.3 \pm 3.2$	3
48	$3.6 \pm 1.1$	$7.4 \pm 3.6$	3
49	$4.9 \pm 1.1$	$10.9 \pm 3.6$	4
50	$7.4 \pm 2.4$	$14.1 \pm 3.4$	4
51	$7.8 \pm 1.8$	$11.5 \pm 7.6$	5
52	$8.9 \pm 1.1$	$9.5 \pm 1.1$	4
53	$13.9 \pm 5.0$	$14.5 \pm 5.3$	4
54	$22.4 \pm 2.9$	$23.1 \pm 3.0$	5
55	$31.8 \pm 3.3$	$32.8 \pm 3.2$	5
56	$38.6 \pm 9.0$	$44.5 \pm 10.7$	5
57	$67.1 \pm 10.9$	$72.5 \pm 17.1$	5
58	$246.9 \pm 74.1$	$278.7 \pm 77.6$	6
59	$313.4 \pm 46.0$	$348.2 \pm 104.3$	6

\*Negative values are indicative of a crystallization process during the cooling step

SR-XRD was also employed to determine nucleation time at the chosen temperatures of 42, 44, 46, 48, 50, 52, 53, 55, 56 and  $57\text{ }^{\circ}\text{C}$ , as summarized in Table 3. Nucleation time was described as  $t_{\text{onset}}$ , as it was determined as the precise moment at which corresponding SR-SAXD peak was firstly detected.

No experimental error was associated with the SR-XRD measurements, due to the impossibility to perform repetitions for each experimental condition. Most of the related SR-XRD patterns are shown as supplementary material in Fig. S1-S6, and here we present a selection (Figs. 2–5) for isotherms at the chosen temperatures depicted in Fig. 1.

As confirmed by SR-XRD data, when PPP was rapidly cooled to a temperature within the range from 40 to  $46\text{ }^{\circ}\text{C}$ , the polymorphic crystallization was directed to obtain metastable  $\alpha$  form. As an example, Fig. 2 (see also Fig. S1) shows related SR-SAXD and SR-WAXD patterns obtained when PPP was set at a temperature of  $42\text{ }^{\circ}\text{C}$  until complete crystallization and consequently heated at  $2\text{ }^{\circ}\text{C min}^{-1}$ .

Soon after the temperature of  $42\text{ }^{\circ}\text{C}$  was reached, double chain-length structure (2L) SR-SAXD peak at  $4.5\text{ nm}$ ,

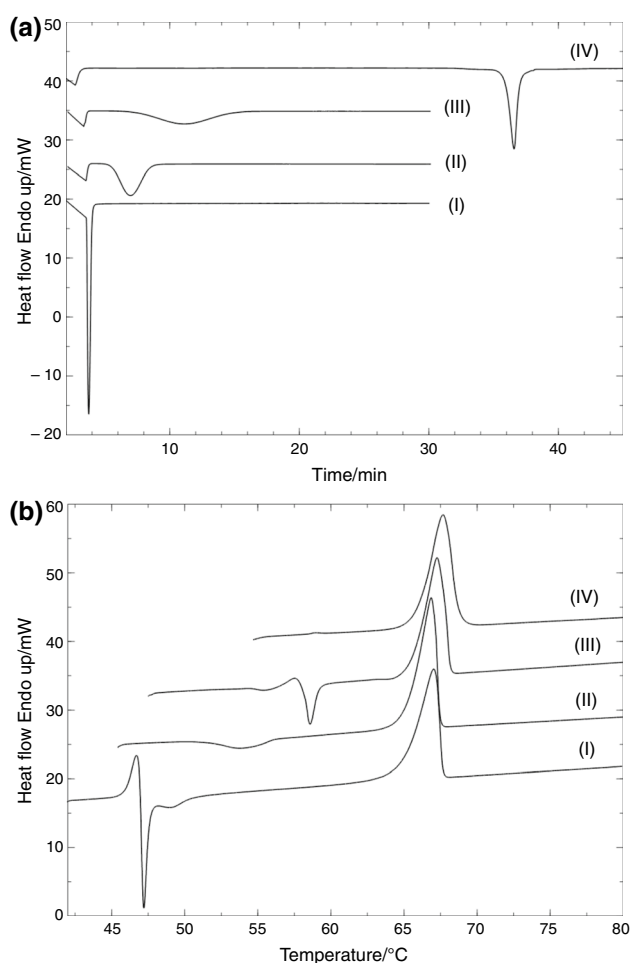


**Fig. 1** DSC curves obtained during **a** the isothermal step, and **b** succeeding heating of PPP to 80 °C at 2 °C min<sup>-1</sup>. Curves (I), (II), (III) and (IV) correspond to DSC experiments with setting temperatures of 42, 46, 48 and 55 °C, respectively

**Table 3** Nucleation time of PPP determined by SR-XRD at different crystallization temperatures between 40 and 59 °C

$T_c/^\circ\text{C}$	$t_{\text{onset}}/\text{min}$
42	0
44	0
46	0.5; 1.5
48	2
50	2
52	4
53	13
55	30.5
56	41
57	64

associated with typical SR-WAXD peak of  $\alpha$  form at 0.42 nm, was identified. Thus, we determined a  $t_{\text{onset}}$  for  $\alpha$  nucleation of 0 min through this technique (Table 3), which

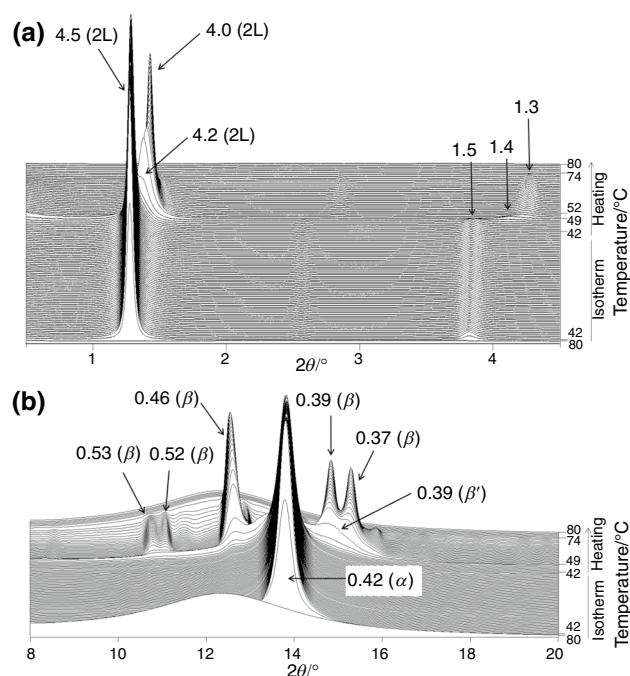


**Fig. 2** **a** SR-SAXD, and **b** SR-WAXD patterns of PPP when quickly cooled to 42 °C, kept for 30 min ( $\alpha$  crystallization), and heated to 80 °C at 2 °C min<sup>-1</sup>

is in accordance with the nucleation time determined by DSC of  $0.1 \pm 0.2$  min (Table 2).

When heated, SR-XRD patterns showed a progressive decrease in intensity of  $\alpha$  peaks and, at a temperature of about 49 °C, a gradual increase in 2L peaks at 4.2 and 0.39 nm, corresponding to  $\beta'$  form. Following, the SR-SAXD peak at 4.2 nm shifted to 4.0 nm, and  $\beta$ -type SR-WAXD reflections were detected at 0.53, 0.52, 0.46, 0.39 and 0.37 nm.

By combining these results with corresponding DSC heating data (curve (I) in Fig. 1b), one may assume that a melt-mediated polymorphic transformation occurred from  $\alpha$  to  $\beta'$  (melting endothermic peak with  $T_{\text{onset}}$  at 45.9 °C and exothermic crystallization signal for  $\beta'$  with  $T_{\text{peak}}$  at 47.2 °C), which soon after transformed into  $\beta$  form (exothermic peak with top temperature of 49.2 °C). SR-XRD reflections caused by the most stable form completely vanished at 74 °C (endothermic DSC event with onset temperature of 64.7 °C). Kellens et al. [12] did not observe the occurrence of  $\beta'$  form as intermediate phase during the polymorphic transformation from  $\alpha$  to  $\beta$  by using laboratory-scale X-ray diffraction techniques. Only synchrotron radiation experiments seemed to reveal a possible involvement of this unstable intermediate [9]. Here, by also using synchrotron radiation, we confirmed the intermediate role of  $\beta'$  when obtaining  $\beta$  from  $\alpha$  form, although it was detected during a very short period of time. Nevertheless, at distinct experimental conditions,  $\beta'$  form

could not be discerned even if synchrotron radiation was employed (see Fig. S1).

Concurrent crystallization of  $\alpha$  and  $\beta'$  forms occurred for a crystallization temperature of 46 °C. As shown in the enlarged inserted image in Fig. 3a, the SR-SAXD peak at 4.5 nm ( $\alpha$  form) was firstly spotted 0.5 min after reaching the setting temperature, whereas that characteristic of  $\beta'$  form appeared 1 min later, that is 1.5 min after the beginning of the isothermal step. These events were coordinated with the almost simultaneous occurrence of  $\alpha$  (0.42 nm) and  $\beta'$  (0.43, 0.42 and 0.39 nm) reflections in corresponding SR-WAXD patterns (Fig. 3b).

Then, according to synchrotron data, for a crystallization temperature of 46 °C, we determined two nucleation times: one for  $\alpha$  (0.5 min) and another one for  $\beta'$  (1.5 min) (Table 3). However, these two polymorphic crystallization processes could not be discerned by DSC, as a single well-defined exothermic event was solely observed, defining a  $t_{\text{onset}}$  of  $2.0 \pm 1.1$  min (Table 2).

The DSC information for the heating procedure at  $2\text{ °C min}^{-1}$  after complete crystallization of  $\alpha$  and  $\beta'$  (curve (II) in Fig. 1b) showed a flat exothermic phenomenon with  $T_{\text{onset}}$  of 51.2 °C and  $T_{\text{peak}}$  of 53.9 °C which, based on the SR-XRD data, corresponded to the polymorphic transition of  $\alpha$  and  $\beta'$  to most stable  $\beta$  (4.0 nm; and 0.53, 0.52, 0.46, 0.39 and 0.37 nm), which finally melted at 64.9 °C ( $T_{\text{onset}}$  of the last endothermic event in curve (II) of Fig. 1b).

This concurrent crystallization of  $\alpha$  and  $\beta'$  forms did not take place at higher temperatures, so that  $\beta'$  was the only phase detected when PPP was rapidly cooled to 48 °C. At these conditions, we determined a nucleation time of  $3.6 \pm 1.1$  min (Table 2) by DSC and of 2 min by SR-XRD (Table 3 and enlarged image in Fig. 4a).

$\beta'$  phase was identified through its characteristic SR-WAXD peaks at 0.43, 0.42 and 0.39 nm and, when heated, it transformed into  $\beta$  (with long- and short-spacing values of 4.0 nm; and 0.53, 0.52, 0.46, 0.39 and 0.38 nm, respectively) at about 61 °C. This polymorphic transition was assigned to the melt-mediated transformation shown in the associated DSC heating curve ((III) in Fig. 1b), consisting of an endothermic melting peak with  $T_{\text{onset}}$  of 56.3 °C and exothermic crystallization event with maximum value of 58.6 °C. Melting temperature of  $\beta$  form was about 65.3 °C (onset), and at 75 °C no SR-XRD peaks were longer observed. The  $\beta'$  polymorph was the one crystallizing at temperatures from 48 to 53 °C (included), as demonstrated in Fig. S2-S4.

The polymorphic behavior was significantly simplified when increasing the setting temperature, so that at 55 °C molten PPP directly crystallized into most stable  $\beta$ . However, the nucleation time was also meaningfully increased to  $31.8 \pm 3.3$  min, according to the DSC results (Table 2), or to 30.5 min, based on the SR-XRD measurements, as shown in Table 3 and insert in Fig. 5a. Thus, most stable  $\beta$  form was identified through its 2L structure SR-SAXD peak

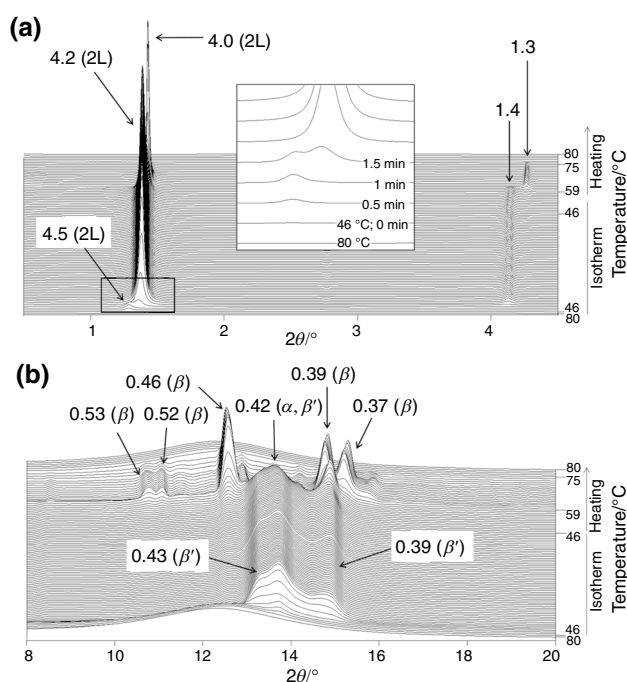


**Fig. 3** **a** SR-SAXD, and **b** SR-WAXD patterns of PPP when quickly cooled to 46 °C, kept for 30 min ( $\alpha + \beta'$  crystallization), and heated to 80 °C at  $2\text{ °C min}^{-1}$

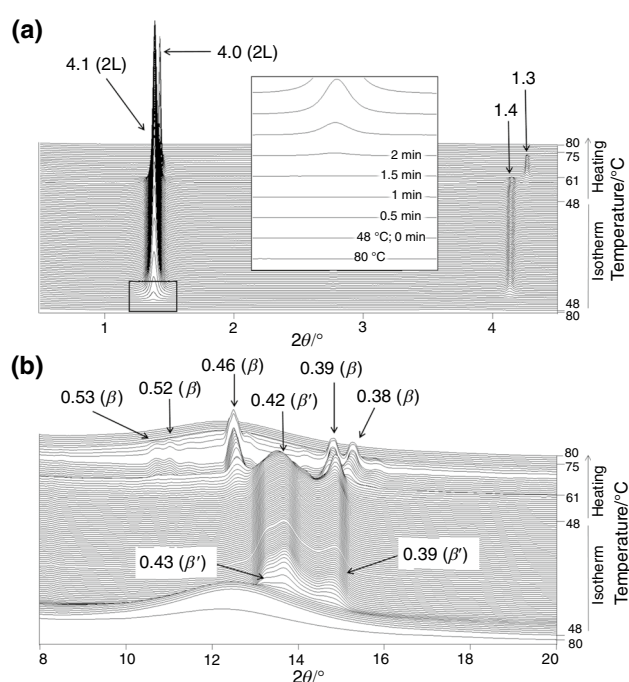


**Fig. 4** **a** SR-SAXD, and **b** SR-WAXD patterns of PPP when quickly cooled to 48 °C, kept for 30 min ( $\beta'$  crystallization), and heated to 80 °C at  $2\text{ °C min}^{-1}$

at 4.0 nm and characteristic short-spacing values of 0.53, 0.52, 0.46, 0.39 and 0.38 nm (SR-WAXD pattern in Fig. 5b). When heated, this form simply melted at 65.7 °C ( $T_{\text{onset}}$ ), as shown in the heating curve (IV) in Fig. 1b. We identified the occurrence of  $\beta$  form at higher temperatures of 56 and 57 °C and determined higher nucleation times of 41 and 64 min, respectively, by SR-XRD (Fig. S5 and S6).

By comparing the last endothermic DSC event assigned to the melting process of  $\beta$ , one may note that their onset, peak top and end temperatures increased from curve (I) (in which  $\alpha$  crystallized during the isotherm) to curve (III) ( $\beta'$  crystallization during the setting) and curve (IV) (crystallization of most stable  $\beta$ ). In more detail, onset temperature values for curves (I) to (IV) were 64.7, 64.9, 65.3 and 65.7 °C, peak top temperatures were 66.9, 67.1, 67.3 and 67.7 °C, and we also determined an increase in end temperatures as follows: 67.5, 67.7, 68.2 and 68.8 °C. This could be due to the presence of more than one  $\beta$  form (e.g.,  $\beta_2$  and  $\beta_1$ ), as determined by previous studies.

As previously stated, Takeguchi et al. [18] described the occurrence of four different  $\beta$  forms for PPP depending on the thermal route to which samples were subjected. They observed slight differences in melting temperatures but similar polymorphism with the same subcell packing. By contrast, previous work by Kellens et al. [9], determined that the differences observed were not due to the existence of multiple  $\beta$  forms. They concluded that the thermal history applied to PPP may involve the removal of some imperfections in polymorphic forms during certain phase transformations, and so leading to different degrees of crystallinity and crystalline perfection. Then, as in the present work we did not determine variations in SR-XRD patterns, demonstrating the occurrence or coexistence of multiple  $\beta$  forms, we did not make the distinction and used  $\beta$  as a general term.

Nucleation times for  $\alpha$ ,  $\beta'$  and  $\beta$  forms of PPP are depicted in Fig. 6, in which dots and triangles represent those determined by DSC and SR-XRD measurements, respectively.

Nucleation time values exhibited an exponential growth type and, as previously stated, error bars associated with the DSC data, and so the dispersion of nucleation time and amount of analyses performed, increased as the setting temperature increased. However, even if just one SR-XRD experiment was carried out for each experimental condition, there was a good agreement between the results obtained by the two techniques. The small differences spotted may mostly be due to the different sample environment (e.g., sample cell) and the amount of sample employed.

These results do not totally agree with those previously reported by Kellens et al. [12] on the isothermal crystallization of PPP at different temperatures. They carried out laboratory-scale XRD experiments ex situ, not in situ, by previously controlling the sample temperature in a hot stage and, once crystallized, obtaining XRD data at room

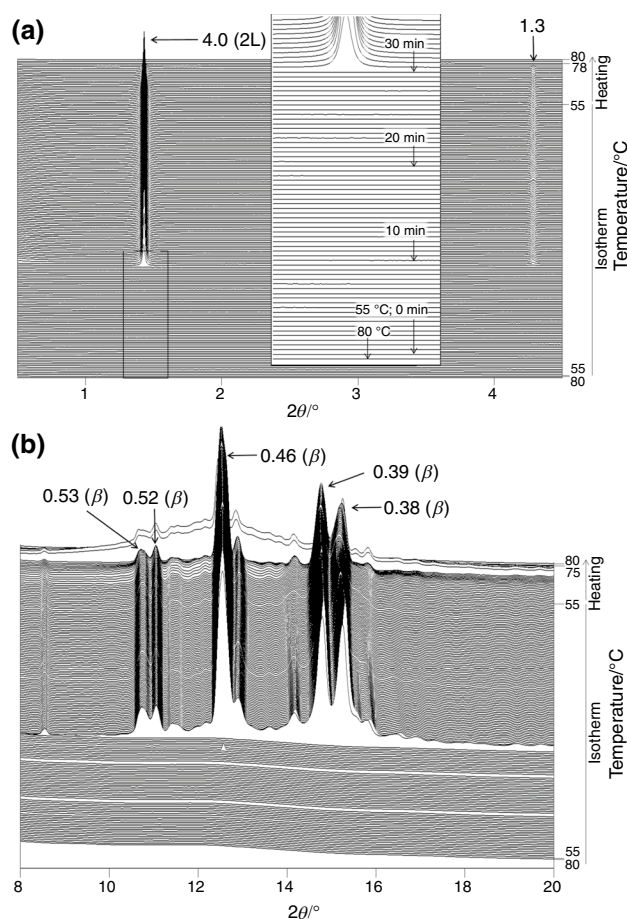


**Fig. 5** **a** SR-SAXD, and **b** SR-WAXD patterns of PPP when quickly cooled to 55 °C, kept for 75 min ( $\beta$  crystallization), and heated to 80 °C at 2 °C min<sup>-1</sup>

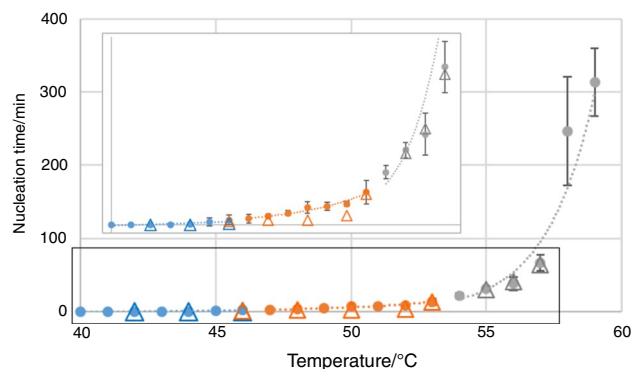


**Fig. 6** Nucleation time (min) for  $\alpha$  (blue),  $\beta'$  (orange), and  $\beta$  (gray) at the different setting temperatures examined within the range from 40 to 59 °C, determined by DSC (dots) and SR-XRD (triangles). DSC data include corresponding error bars

temperature. At such conditions, they observed concurrent crystallization of  $\alpha$  and  $\beta'$  form at 43 °C and solely  $\beta'$  was formed in the temperature range from 44 to 49.5 °C. Most

stable  $\beta$  form started to be detected at crystallization temperatures of 50 °C, with coexistence with  $\beta'$  (detected by DSC) until a temperature of 54 °C, and only  $\beta$  at temperatures above 55 °C.

In this study, we detected the occurrence of the different polymorphs at lower temperatures compared to Kellens' work. In more detail,  $\alpha$  was formed at  $T_c$  from 40 to 46 °C, temperature at which coexisted with  $\beta'$ , and  $\beta'$  was solely detected from 47 to 53 °C. Then, most stable  $\beta$  crystallized at temperatures of 54 °C and higher. The fact that Kellens' and co-authors determined the occurrence of all polymorphic forms at lower temperatures may be related to the acquisition of XRD data at room temperature after isothermal crystallization carried out in a hot stage device. If crystallization processes had not completely finish when cooled at room temperature, probably this change in temperature may have accelerated some crystallization phenomena. The authors also determined induction time for crystallization processes of the different phases, and observed a dramatic change, probably related to the  $\beta$  form occurrence, at 50 °C, temperature at which induction time significantly decreased compared to lower setting temperatures, and induction time became even lower for  $T_c$  of 51 and 52 °C. In the present work, we did not observe such a jump, and we believe that it may be associated with the increase in values dispersion, and so the wideness of related error bars, as  $T_c$  increased. Nucleation becomes

a stochastic process, and for this reason in the present work, as previously noted, we increased the amount of DSC experiments performed as the setting temperature was higher, due to the increase in dispersion in nucleation time values. Furthermore, we observed a good correlation with nucleation time values determined by DSC and SR-XRD.

### PPP crystallization under dynamic conditions

The crystallization, transformation and melting behavior of pure monoacid PPP was also evaluated during thermal treatments consisting of (1) cooling and reheating at a high rate of 15 °C min<sup>-1</sup>, (2) cooling and reheating at an intermediate rate of 2 °C min<sup>-1</sup>, (3) cooling and reheating at 0.5 °C min<sup>-1</sup>, and (4) cooling at 0.1 °C min<sup>-1</sup> and reheating at 2 °C min<sup>-1</sup>.

As a summary, Table 4 shows DSC data for crystallization, transformation and melting processes observed when PPP was cooled and heated at the varied rates.

Unless otherwise indicated,  $T_{\text{onset}}$  will be used to define the temperature of thermal events. In addition, TOPLM experiments were carried out under some conditions to monitor microstructural changes occurring in the TAG sample during polymorphic changes.

**Table 4** DSC data of the polymorphic crystallization and transformation behavior of PPP when cooled and subsequently heated at different rates

	Cooling at 15 °C min <sup>-1</sup>		Heating at 15 °C min <sup>-1</sup>			
	$\alpha$ (c)	$\alpha \rightarrow \text{sub-}\alpha$	sub- $\alpha \rightarrow \alpha$	$\alpha$ (m)	$\beta'$ (c)/ $\beta' \rightarrow \beta$	$\beta$ (m)
$T_{\text{onset}}/^\circ\text{C}$	41.2 ± 0.4	n.d	n.d	44.5 ± 0.4	48.4 ± 0.6	63.2 ± 0.5
$\Delta H/J \text{ g}^{-1}$	-118 ± 16			80 ± 11	-144 ± 23	189 ± 22
	Cooling at 2 °C min <sup>-1</sup>		Heating at 2 °C min <sup>-1</sup>			
	$\alpha + \beta'$ (c)	$\alpha$ (m)	$\beta'$ (c)	$\beta' \rightarrow \beta$	$\beta$ (m)	
$T_{\text{onset}}/^\circ\text{C}$	43.7 ± 0.7	45.5 ± 0.7	46.6 ± 0.8	47.4 ± 0.8		64.6 ± 0.7
$\Delta H/J \text{ g}^{-1}$	-125 ± 4	33 ± 2	-91 ± 5 <sup>a</sup>			203 ± 6
	Cooling at 0.5 °C min <sup>-1</sup>		Heating at 0.5 °C min <sup>-1</sup>			
	$\beta'$ (c)		$\beta' \rightarrow \beta$		$\beta$ (m)	
$T_{\text{onset}}/^\circ\text{C}$	44.5 ± 0.3		45.7 ± 0.3		65.3 ± 0.2	
$\Delta H/J \text{ g}^{-1}$	-137 ± 9		-19 ± 4		206 ± 6	
	Cooling at 0.1 °C min <sup>-1</sup>		Heating at 2 °C min <sup>-1</sup>			
	$\beta$ (c)		$\beta$ (m)			
$T_{\text{onset}}/^\circ\text{C}$	53.4 ± 1.4		65.7 ± 0.5			
$\Delta H/J \text{ g}^{-1}$	-185 ± 7		211 ± 6			

(c): crystallization; (m): melting; n.d.: not determined. <sup>a</sup> $\Delta H$  corresponds to the global enthalpy of the overlapped phenomena

### Cooling from the melt and reheating at a high rate of $15\text{ }^{\circ}\text{C min}^{-1}$

DSC and SR-XRD data obtained when PPP was cooled from the melt to  $-80\text{ }^{\circ}\text{C}$  and subsequently heated at  $15\text{ }^{\circ}\text{C min}^{-1}$  is shown in Fig. 7a and b, respectively.

Upon cooling, a single exothermic signal was detected at  $T_{\text{onset}}$  of  $41.2\text{ }^{\circ}\text{C}$  by DSC. Diffraction peaks at  $4.5\text{ nm}$  in the SR-SAXD and  $0.41\text{ nm}$  in the SR-WAXD patterns allowed to confirm the crystallization of  $\alpha$  form. No additional polymorphic phenomena occurred during the cooling step according to DSC data but a weak reflection with d-spacing of  $0.38\text{ nm}$  was detected in SR-WAXD data almost at the end of cooling. This was due to the change from a hexagonal to a pseudo-hexagonal subcell typically shown by TAGs with diverse composition, symmetry, and degree of unsaturation during  $\alpha \rightarrow \text{sub-}\alpha$  transitions at sub-zero temperatures [12, 19]. When reheating, the  $\text{sub-}\alpha \rightarrow \alpha$  transformation was followed by the melting of  $\alpha$ , which by DSC was spotted at  $44.5\text{ }^{\circ}\text{C}$ . Afterward, a broad exothermic peak corresponding to several polymorphic events, which were identified by synchrotron data, appeared at  $48.4\text{ }^{\circ}\text{C}$ . Thus, at  $58\text{ }^{\circ}\text{C}$  the intensity of the  $\alpha$  peak at  $4.5\text{ nm}$  decreased at the expense of a new one at around  $4.2\text{ nm}$  in SR-SAXD, whereas the occurrence of a new signal at  $0.38\text{ nm}$  in SR-WAXD indicated the crystallization of  $\beta'$ . SAXD peaks corresponding to  $\alpha$  and  $\beta'$  were no longer observed when reaching  $62\text{ }^{\circ}\text{C}$ , and emerging peaks at  $0.46$ ,  $0.39$ , and  $0.37\text{ nm}$  confirmed the transformation of metastable  $\beta'$  form into  $\beta$ , which finally melted at  $63.2\text{ }^{\circ}\text{C}$ .

These fast-heating conditions applied did not permit to clarify the polymorphic transformation pathway followed by PPP during the  $\beta'$  transformation due to overlapping of DSC thermal signals. Monitoring of  $\beta'$  development and transformation by SR-XRD was also hindered by the  $5\text{ }^{\circ}\text{C}$  difference between successive patterns. Figure 8 depicts the TOPLM micrographs taken during the heating treatment of  $\alpha$  crystals at  $15\text{ }^{\circ}\text{C min}^{-1}$ .

The liquid medium originated in the sample due to the  $\alpha$  melting was still present after  $\beta'$  crystals were obtained and during the microstructural changes related to the  $\beta' \rightarrow \beta$  transition. Despite the lack of confirmation, the conversion of  $\beta'$  into  $\beta$  through the melt would agree with previous XRD, DSC, and microscopy studies on the transformation behavior of PPP  $\beta'$  isothermally crystallized. During heating processes at  $1\text{ }^{\circ}\text{C min}^{-1}$ ,  $\beta'$  transformed into  $\beta$  via melt-mediation at temperatures ranging from  $52$  to  $60.5\text{ }^{\circ}\text{C}$  depending on the perfection in molecular packing allowed by the crystallization conditions [13, 20].

In line with this, one explanation for the short-life exhibited by  $\beta'$  through SR-XRD patterns may be the low stability

induced by a rapid and less perfect molecular packing under rapid heating. This would favor the quick transformation of  $\beta'$  into  $\beta$  soon after recrystallizing from the  $\alpha$  melt. It cannot be ruled either that some  $\beta$  formed directly from the  $\alpha$  melt when reaching elevated temperatures close to that of  $\beta'$  melting.

### Cooling from the melt and reheating at intermediate and low rates

PPP cooled at  $2\text{ }^{\circ}\text{C min}^{-1}$  showed the concurrent crystallization of  $\alpha$  and  $\beta'$  at  $43.7\text{ }^{\circ}\text{C}$  (Fig. 7c and d). When reheating at the same rate, a set of close events involving a first endothermic peak followed by two consecutive exothermic signals were detected by DSC. The strengthening of the peak at  $4.2\text{ nm}$  at the expense of that at  $4.5\text{ nm}$  in the small-angle region of laboratory-scale XRD patterns (Fig. 7d, left) at  $45\text{ }^{\circ}\text{C}$  indicated that  $\alpha$  form melted first and, soon after,  $\beta'$  crystallized. The second exothermic DSC peak at around  $47\text{ }^{\circ}\text{C}$  was due to the  $\beta' \rightarrow \beta$  solid–solid transformation. At a close temperature, the small-angle reflection had shifted toward a d-spacing of  $4.1\text{ nm}$ , and highly intense typical  $\beta$  wide-angle peaks emerged (denoted by ■). Finally, stable  $\beta$  form melted at around  $65\text{ }^{\circ}\text{C}$ .

For PPP cooled at  $0.5\text{ }^{\circ}\text{C min}^{-1}$  (see Fig. 7e and f), laboratory-scale XRD confirmed the sole occurrence of  $\beta'$  (reflections at  $0.43$ ,  $0.42$  and  $0.38\text{ nm}$ ). During reheating, the solid-state transformation of this form into most stable  $\beta$  before complete melting resulted in the double exothermic thermal event starting at  $45.7\text{ }^{\circ}\text{C}$ . When lowering the speed of cooling to  $0.1\text{ }^{\circ}\text{C min}^{-1}$ , single sharp exothermic and endothermic episodes related to the crystallization and melting of  $\beta$  took place throughout the whole thermal treatment (Fig. 7g and 7h).

The results here confirmed by XRD are in agreement with previous data on PPP obtained by Himawan et al. [21]. Based on the  $\Delta H$  and the characteristic temperatures of DSC peaks obtained during cooling, the authors suggested that the occurrence of  $\alpha$  was promoted at cooling rates from  $20$  to  $2.5\text{ }^{\circ}\text{C min}^{-1}$ , under which concurrent crystallization of  $\alpha$  and  $\beta'$  took place. Moreover, only when cooling rates of  $0.2\text{ }^{\circ}\text{C min}^{-1}$  and below were employed, enough time was provided to allow the nucleation and subsequent growth of the  $\beta$  phase. The occurrence of the intermediate  $\beta'$  form of PPP during  $\alpha \rightarrow \beta$  transformations has been overlooked in several studies solely based on thermal analysis [21, 22]. Our results show that the latter occurs during thermal processing when applying from intermediate to fast-heating rates. They also evidence the important complementary role of powerful identification techniques, such as XRD (in situ both laboratory-scale and synchrotron radiation source), to

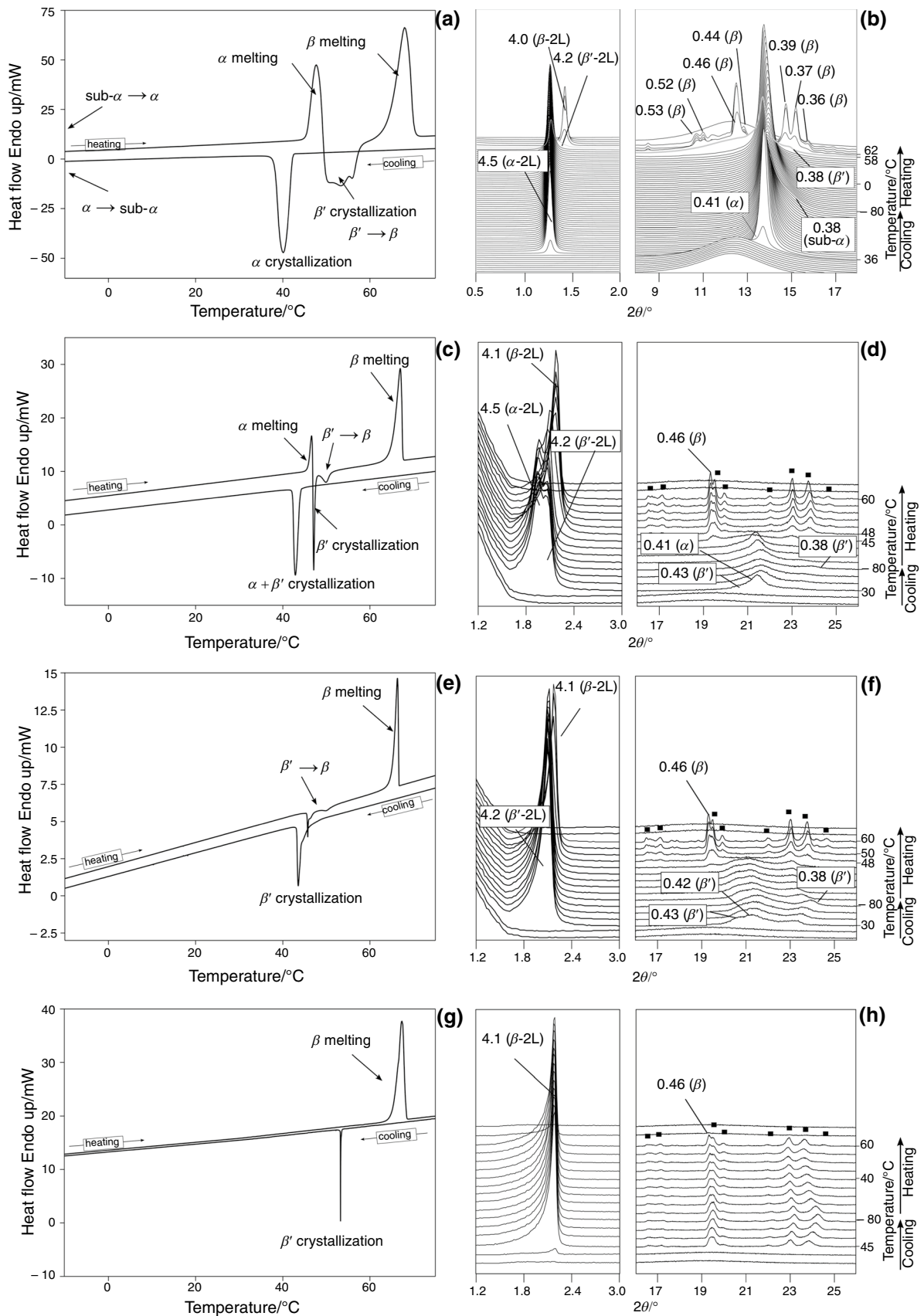


**Fig. 7** DSC curves (left) and XRD data (right) of PPP when cooled and subsequently heated at different rates. **a, b** Cooling and heating at  $15\text{ }^{\circ}\text{C min}^{-1}$ ; **c, d** Cooling and heating at  $2\text{ }^{\circ}\text{C min}^{-1}$ ; **e, f** Cooling and heating at  $0.5\text{ }^{\circ}\text{C min}^{-1}$ ; and **g, h** Cooling at  $0.1\text{ }^{\circ}\text{C min}^{-1}$  and heating at  $2\text{ }^{\circ}\text{C min}^{-1}$ . ■ denotes characteristic wide-angle peaks of PPP  $\beta$  form.  $d$ -spacing values are given in nm

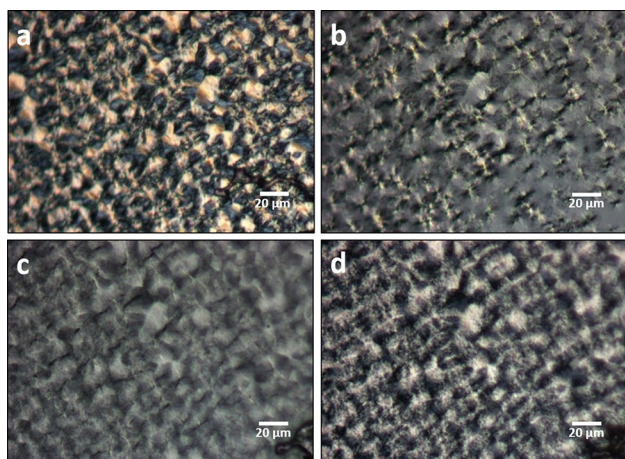


**Fig. 8** Polarized light micrographs of PPP obtained during heating at  $15\text{ }^{\circ}\text{C min}^{-1}$  soon after a melt cooling process at the same rate. **a**  $\alpha$  spherulites at  $38\text{ }^{\circ}\text{C}$ ; **b**  $\alpha$  melting at  $46\text{ }^{\circ}\text{C}$ ; **c**  $\beta'$  crystals + liquid at  $51\text{ }^{\circ}\text{C}$ ; and **d**  $\beta$  crystals + liquid at  $60\text{ }^{\circ}\text{C}$

obtain a more accurate picture of the polymorphic behavior of lipid systems.

Figure 9 summarizes the overall crystallization, transformation, and melting behavior determined for PPP.

As shown, the occurrence of the least stable polymorph was favored by the application of a high cooling rate, whereas decreasing the speed promoted the nucleation and growth of more stable forms. During reheating, polymorphs obtained under the different conditions transformed into the next one in order of increasing thermodynamic stability until reaching  $\beta$  form in all cases. One may note that the melting temperature of this most stable form progressively increased from  $63.2$  to  $65.7\text{ }^{\circ}\text{C}$  when changing the thermal program applied from high to low cooling and heating rates (see Table 4). Concurrently, enthalpy values associated with this melting process also slightly increased from  $189$  to  $211\text{ J g}^{-1}$ . However, these variations became significant when comparing the data obtained for cooling/heating at  $15/15\text{ }^{\circ}\text{C min}^{-1}$  and at  $2/2\text{ }^{\circ}\text{C min}^{-1}$ , but the deviation observed may be within experimental error at the experimental conditions of  $0.5/0.5\text{ }^{\circ}\text{C min}^{-1}$  and  $0.1/2\text{ }^{\circ}\text{C min}^{-1}$ . The lowest  $T_{\text{onset}}$  assigned to the  $\beta$  form melting for the experiment held at  $15/15\text{ }^{\circ}\text{C min}^{-1}$  could be due to the presence of some remaining metastable  $\beta'$  form. This is in agreement with the rapid and continuous polymorphic transformation processes which occurred when heating at  $15\text{ }^{\circ}\text{C min}^{-1}$ ,

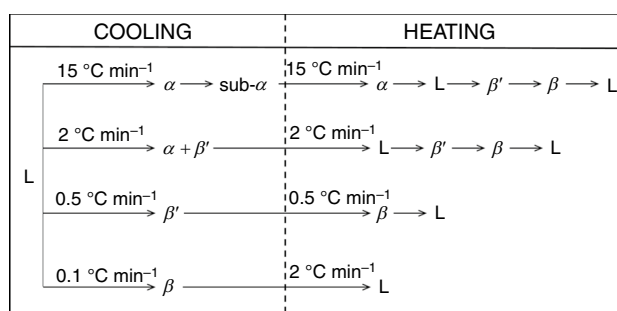


**Fig. 9** Summary of polymorphic crystallization and transformation pathways of PPP under varied cooling and heating rates

as  $\beta$  form melted soon after it was obtained from metastable  $\beta'$ . By contrast, at lower cooling and heating rates, the  $\beta' \rightarrow \beta$  phase transition occurred at least  $10\text{ }^{\circ}\text{C}$  before the  $\beta$  melting, which may imply a more isolated  $\beta$  form with a sharper melting signal (Fig. 7).

The crystallization behavior shown by these TAGs did not comply with the Ostwald step rule of stages, which states that least stable polymorphs, with closest thermodynamic properties to the parent phase, tend to form first during crystallization, and then transform sequentially into the next one until achieving the most stable configuration [23, 24]. This is in line with previous research on pure TAGs, their mixtures, and more complex lipids subjected to the influence of external factors [3, 25–29].

## Conclusions

The combined usage of DSC and in situ XRD, with laboratory-scale and synchrotron radiation source, allowed to determine the crystallization behavior of PPP under isothermal and dynamic conditions, based on the variation of the cooling and heating rates. Nucleation time for the different polymorphs ( $\alpha$ ,  $\beta'$  and  $\beta$ ) displayed an exponential growth type, and the dispersion of the values for the same isothermal experiment increased as setting temperature increased, due to the stochastic nature of nucleation phenomena. The higher difficulty to crystallize for a more ordered, compact and stable polymorphic phase may also contribute to the dispersion in crystallization time. The slight differences observed between DSC and SR-XRD data may be due to the different set-up of the sample required by the two techniques. Experiments based on dynamic thermal treatments showed the predominance of more stable forms when decreasing the rate of cooling. However, most stable  $\beta$  form was reached during the heating step at all the experimental conditions examined.

**Supplementary Information** The online version contains supplementary material available at <https://doi.org/10.1007/s10973-024-13196-3>.

**Acknowledgements** The authors acknowledge the Generalitat de Catalunya through project 2021 SGR 00262, and the financial support of Grant PID2019-107032RB-I00 funded by MCIN/AEI/<https://doi.org/10.13039/501100011033/>. Funding from the ALBA synchrotron facility is also gratefully acknowledged. SR-XRD experiments were performed with the approval of the ALBA Scientific Advisory Committee (proposals 2020074400 and 2017022003). The authors thank Dr. Marc Malfois, responsible for the BL11-NCD-SWEET at ALBA, for his assistance.

**Author contributions** All authors contributed to the experimental design. Experiments, data acquisition and analyses were carried out by LB-G and JM. The original draft of the manuscript was prepared by LB-G. Funding acquisition was done by LB-G. and TC Manuscript review was performed by TC and KS.

**Funding** Open Access funding provided thanks to the CRUE-CSIC agreement with Springer Nature.

## Declarations

**Conflict of interest** The authors have no competing interests to declare that are relevant to the content of this article.

**Open Access** This article is licensed under a Creative Commons Attribution 4.0 International License, which permits use, sharing, adaptation, distribution and reproduction in any medium or format, as long as you give appropriate credit to the original author(s) and the source, provide a link to the Creative Commons licence, and indicate if changes were made. The images or other third party material in this article are included in the article's Creative Commons licence, unless indicated otherwise in a credit line to the material. If material is not included in the article's Creative Commons licence and your intended use is not permitted by statutory regulation or exceeds the permitted use, you will need to obtain permission directly from the copyright holder. To view a copy of this licence, visit <http://creativecommons.org/licenses/by/4.0/>.

## References

- Larsson K, Quinn P, Sato K, Tiberg F. Lipids: structure, physical properties and functionality. Bridgewater: The Oily Press; 2006.
- Sato K. Solidification and phase transformation behaviour of food fats - a review. *Fett-Lipid*. 1999. [https://doi.org/10.1002/\(SICI\)1521-4133\(199912\)101:12%3c467::AID-LIPI467%3e3.0.CO;2-D](https://doi.org/10.1002/(SICI)1521-4133(199912)101:12%3c467::AID-LIPI467%3e3.0.CO;2-D).
- Sato K. Crystallization behaviour of fats and lipids—a review. *Chem Eng Sci*. 2001. [https://doi.org/10.1016/S0009-2509\(00\)00458-9](https://doi.org/10.1016/S0009-2509(00)00458-9).
- Basso RC, Paula A, Ribeiro B, Helen M, Antonio L, Guaraldo LA, Oliveira A, Pavie L, Grimaldi R. Tripalmitin and monoacylglycerols as modifiers in the crystallisation of palm oil. *Food Chem*. 2010. <https://doi.org/10.1016/j.foodchem.2010.03.113>.
- Vereecken J, Foubert I, Smith KW, Dewettinck K. Effect of Sat-SatSat and SatOSat on crystallization of model fat blends. *Eur J Lipid Sci Technol*. 2009. <https://doi.org/10.1002/ejlt.200800150>.
- Vereecken J, Foubert I, Smith KW, Sassano GJ, Dewettinck K. Crystallization of model fat blends containing symmetric and asymmetric monounsaturated triacylglycerols. *Eur J Lipid Sci Technol*. 2010. <https://doi.org/10.1002/ejlt.200900037>.
- Vereecken J, de Graef V, Smith KW, Wouters J, Dewettinck K. Effect of TAG composition on the crystallization behaviour of model fat blends with the same saturated fat content. *Food Res Int*. 2010. <https://doi.org/10.1016/j.foodres.2010.06.008>.
- Sato K, Kuroda T. Kinetics of melt crystallization and transformation of tripalmitin polymorphs. *J Am Oil Chem Soc*. 1987. <https://doi.org/10.1007/BF02546266>.
- Kellens M, Meeussen W, Riekel C, Reynaers H. Time resolved X-ray diffraction studies of the polymorphic behaviour of tripalmitin using synchrotron radiation. *Chem Phys Lipids*. 1990. [https://doi.org/10.1016/0009-3084\(90\)90153-I](https://doi.org/10.1016/0009-3084(90)90153-I).
- Hagemann JW, Tallent WH. Differential scanning calorimetry of single acid triglycerides: effect of chain length and unsaturation. *J Am Oil Chem Soc*. 1972. <https://doi.org/10.1007/BF02612641>.
- Simpson TD, Hagemann JW. Evidence of two  $\beta'$  phases in tristearin. *J Am Oil Chem Soc*. 1982. <https://doi.org/10.1007/BF02680269>.
- Kellens M, Meeussen W, Reynaers H. Crystallization and phase transition studies of tripalmitin. *Chem Phys Lipids*. 1990. [https://doi.org/10.1016/0009-3084\(90\)90077-5](https://doi.org/10.1016/0009-3084(90)90077-5).
- Kellens M, Meeussen W, Reynaers H. Study of the polymorphism and the crystallization kinetics of tripalmitin: a microscopic approach. *J Am Oil Chem Soc*. 1992. <https://doi.org/10.1007/BF02636342>.
- Stapley AGF, Himawan C, MacNaughtan W, Foster TJ. A computational method for extracting crystallization growth and nucleation rate data from hot stage microscope images. *Cryst Growth Des*. 2009. <https://doi.org/10.1021/cg9000413>.
- MacNaughtan W, Farhat IA, Himawan C, Starov VM, Stapley AGF. A Differential scanning calorimetry study of the crystallization kinetics of tristearin-tripalmitin mixtures. *J Am Oil Chem Soc*. 2006. <https://doi.org/10.1007/s11746-006-1167-1>.
- Kieffer J, Karkoulis D. PyFAI, a versatile library for azimuthal regrouping. *J Phys Conf Ser*. 2013. <https://doi.org/10.1088/1742-6596/425/20/202012>.
- Kellens M, Meeussen W, Gehrke R, Reynaers H. Synchrotron radiation investigations of the polymorphic transitions of saturated monoacid triglycerides. Part 1: tripalmitin and tristearin. *Chem Phys Lipids*. 1991. [https://doi.org/10.1016/0009-3084\(91\)90119-V](https://doi.org/10.1016/0009-3084(91)90119-V).
- Takeguchi S, Sato A, Hondoh H, Aoki M, Uehara H, Ueno S. Multiple  $\beta$  forms of saturated monoacid triacylglycerol crystals. *Molecules*. 2020. <https://doi.org/10.3390/molecules25215086>.
- Mykhaylyk OO, Martin CM. Effect of unsaturated acyl chains on structural transformations in triacylglycerols. *Eur J Lipid Sci Technol*. 2009. <https://doi.org/10.1002/ejlt.200800183>.
- Stewart DI, Chong PS, Stapley AGF. Investigation of the crystallization and melting of the tripalmitin/triolein system via hot stage microscopy, differential scanning calorimetry, and pulsed NMR. *Cryst Growth Des*. 2017. <https://doi.org/10.1021/acs.cgd.6b01621>.
- Himawan C, MacNaughtan W, Farhat IA, Stapley AGF. Polymorphic occurrence and crystallization rates of tristearin/tripalmitin mixtures under nonisothermal conditions. *Eur J Lipid Sci Technol*. 2007. <https://doi.org/10.1002/ejlt.200600179>.
- Lu C, Zhang B, Zhang H, Guo Y, Dang L, Liu Z, Shu Q, Wang Z. Solid-liquid phase equilibrium and phase behaviors for binary mixtures composed of tripalmitoylglycerol (PPP), 1,3-dipalmitoyl-2-oleoyl-glycerol (POP), and 1,2-dioleoyl-3-palmitoyl-glycerol (POO). *Ind Eng Chem Res*. 2019. <https://doi.org/10.1021/acs.iecr.9b01947>.
- Ostwald W. Studies of the formation and transformation of solid substances. *Zeitschrift Für Phys Chemie*. 1897;22(1):289–330.
- Chung SY, Kim YM, Kim JG, Kim YJ. Multiphase transformation and Ostwalds rule of stages during crystallization of a metal phosphate. *Nat Phys*. 2009. <https://doi.org/10.1038/nphys1148>.

25. Bayés-García L, Calvet T, Cuevas-Diarte MA, Ueno S, Sato K. Crystallization and transformation of polymorphic forms of trioleoyl glycerol and 1,2-dioleoyl-3-*rac*-linoleoyl glycerol. *J Phys Chem B*. 2013. <https://doi.org/10.1021/jp403872a>.
26. Bayés-García L, Calvet T, Cuevas-Diarte MA, Ueno S. In situ crystallization and transformation kinetics of polymorphic forms of saturated-unsaturated-unsaturated triacylglycerols: 1-palmitoyl-2,3-dioleoyl glycerol, 1-stearoyl-2,3-dioleoyl glycerol, and 1-palmitoyl-2-oleoyl-3-linoleoyl glycerol. *Food Res Int*. 2016. <https://doi.org/10.1016/j.foodres.2016.05.011>.
27. Bayés-García L, Calvet T, Cuevas-Diarte MA. Effects of dynamic temperature variations on microstructure and polymorphic behavior of lipid systems. In Sato K (Ed.), *Crystallization of lipids. Fundamentals and applications in food, cosmetics and pharmaceuticals* (pp. 183–210). Hoboken: Wiley-Blackwell, 2018; <https://doi.org/10.1002/9781118593882.ch6>.
28. Bayés-García L, Yoshikawa S, Aguilar-Jiménez M, Ishibashi C, Ueno S, Calvet T. Heterogeneous nucleation effects of talc particles on polymorphic crystallization of cocoa butter. *Cryst Growth Des*. 2022. <https://doi.org/10.1021/acs.cgd.1c00859>.
29. Bayés-García L, Fukao K, Konishi T, Sato K, Taguchi K. Crystallization and transformation behavior of triacylglycerol binary mixtures forming molecular compounds of POP/OPO, POP/*rac*-PPO, and POP/*sn*-PPO. *Cryst Growth Des*. 2023. <https://doi.org/10.1021/acs.cgd.3c00038>.

**Publisher's Note** Springer Nature remains neutral with regard to jurisdictional claims in published maps and institutional affiliations.